J Solid State Electrochem (2005) 9: 174–180
DOI 10.1007/s10008-004-0570-5

ORIGINAL PAPER

De-Sheng Kong · Zhang-Yu Yu · Shi-Ling Yuan

The blocking and structural properties of a Schiff base self-assembled monolayer on the surface of Au(111)

Received: 15 March 2004 / Accepted: 25 March 2004 / Published online: 11 August 2004

Abstract Electrochemistry and in situ electrochemical scanning tunneling microscopy (STM) were used to study the blocking and structural properties of Shiff base V-ape-V self-assembled monolayers (SAMs) on the surface of Au(111) in perchloric acid solution. The complex-plane impedance plots for the SAM covered Au(111) electrodes, with the redox couple of $Fe(CN)_6^{4-/3-}$ present in solution, exhibit arc shapes, revealing that the electrochemical kinetics were controlled by the electron-transfer step. For bare Au(111), the electrode process was mass transport limited. The molecules adsorb on Au(111) with a flat-lying orientation and form a long-range well-defined adlayer. A new structure of $(2\sqrt{3} \times 2\sqrt{7})$ was observed in the double-layer potential region. A structural model is proposed to interpret the molecular registry with Au(111) substrate.

Keywords Cyclic voltammetry · Electrochemical impedance spectroscopy · STM · SAMs · Blocking property

Introduction

The self-assembled monolayer (SAM) approach is a good way to control the surface of electrodes at the molecular level [1, 2, 3, 4]. Their structural and chemical properties make them interesting systems for modifying the electrode/solution interface in a predictable way. Additionally, the preparation of SAMs is simple, and because they are usually on the order of 0.5–10 nm thick, they do not significantly alter the appearance or most other characteristics of the substrate. They have also received considerable attention because of their potential technological application to a variety of areas such as catalysis, corrosion, nano-fabrication, lubrication, and adhesion [5, 6, 7, 8]. Whether the goal of the research is basic or applied science, an understanding of the SAM structure and properties is an essential requirement.

The most popular electrochemical technique used to study redox processes at SAM modified electrodes has been cyclic voltammetry [9, 10, 11] and electrochemical impedance spectroscopy (EIS) [12, 13, 14]. Each technique has its advantages and disadvantages, but EIS has clear advantages because it may provide an efficient separation in frequency domains between diffusion and kinetic control [15, 16]. STM has been used as an important in situ technique for the structural study of adlayers on well-defined electrode surfaces in electrolyte solutions with atomic or molecular resolution [4, 17, 18, 19].

If a coherent monolayer is formed on the electrode, the effect of its thickness, molecular ordering, and dielectric properties on heterogeneous electron transfer may be studied. Alkanethiols on gold, particularly on a Au(111) surface, has become a model system for SAM studies [1, 2, 3], where the strong interaction between gold and sulfur leads to a stable and ordered adlayer upon mere immersion of the gold substrate into a thiol solution. The growth, structure, properties, and applications of alkanethiol SAMs on gold have been widely investigated by various techniques such as electrochemistry [9, 20, 21], spectroscopy [22, 23, 24, 25], scanning probe microscopy (SPM) [26, 27, 28], electron diffraction [29, 30, 31, 32], and theoretical chemistry [33, 34, 35]. Alkanethiol SAMs can suppress faradiac processes such as electrode oxidation and the exchange of electrons between the electrode and solution redox couples. This blocking property is attributed to the densely packed structure of the hydrocarbon chains, which impede the approach of solution ions and molecules to the electrode surface [3, 5].

D.-S. Kong (✉) · Z.-Y. Yu
Department of Chemistry, Qufu Normal University,
273165 Qufu, Shandong, China
E-mail: kongdscn@eyou.com

D.-S. Kong · S.-L. Yuan
Department of Chemistry, Shandong University,
250100 Jinan, Shandong, China

Schiff base SAMs have plenty of promise as protective coatings because they form thin, highly crystalline barrier films on metals such as copper [12, 36, 37, 38, 39] and stainless steel [40], to name a few. Recently, by employing electrochemistry and electrochemical STM, we investigated the SAM of Shiff base V-ape-V formed on Au(111) in 0.1 M $HClO_4$, and found that [41] the adsorption of V-ape-V on Au(111) not only retards the oxidization of Au and reduces the double-layer capacitance, but that it also results in the reconstruction of the Au(111) surface. Two-dimensional ordered molecular arrays with a $\left(5 \times 2\sqrt{3}\right)$ commensurate structure were observed. The V-ape-V molecules are adsorbed on Au(111) in a flat-lying orientation and with a coverage of 1.44 nm^2/molecule.

Herein, we report a new result on V-ape-V SAM formed on Au(111) in acidic solution. The electrochemical behavior of the SAM coated Au(111) electrode was investigated in 1 mM $Fe(CN)^{4-/3-}$ + 0.1 M $HClO_4$ solution by CV and EIS techniques. By using electrochemical STM, it was found that the adsorption of V-ape-V molecules yields an ordered structure with a $\left(2\sqrt{3} \times 2\sqrt{7}\right)$ unit cell structure, which is different from that observed previously as mentioned above.

Experimental

Chemicals and the electrochemical cell

The electrolyte solution, 0.1 M $HClO_4$, was prepared by diluting ultra pure $HClO_4$ (Kanto Chemical Co) with ultra pure Milli-Q water. The structure of the Shiff base V-ape-V used, which was synthesized from ortho-vanilin (Merck Chemical Co.) and other analytic grade reagents as described previously [41], is schematically shown in Scheme 1.

An approximate 100 ml, three-electrode cell was utilized with a platinum-sheet counter electrode and a saturated calomel reference electrode (SCE). Since it is well known that trace chloride ions can be strongly adsorbed on the Au(111) surface, and hence can remarkably enhance the diffusion and promote the dissolution of Au atoms [42, 43], the SCE was connected to the cell via a double-salt-bridge to avoid the diffusion of Cl^- ions into the cell. The electrolyte solutions contain 0.5 mM $K_3Fe(CN)_6$ and 0.5 mM $K_4Fe(CN)_6$ (denoted as 0.1 mM $Fe(CN)_6^{4-/3-}$ in the following), and were deaerated by bubbling highly purified nitrogen gas through them for at least 20 min before use. All experiments were carried out at ambient temperature (20 ± 2 °C).

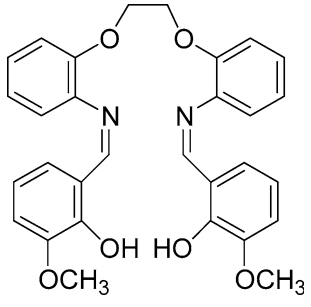

Scheme 1 Molecular structure of Schiff base V-ape-V used as an adsorbate in this work

Electrochemical measurements

The working electrode for electrochemical measurements was a hemispherical single-crystal Au(111) electrode. Before use, it was cleaned by soaking in a Piranha solution (98% H_2SO_4:30% H_2O_2 = 7:3, V/V) for 15–20 min, and washed with ultrapure Milli-Q water thoroughly. Then it was either directly used as a bare electrode, or immersed in an ethanolic solution of V-ape-V (~0.1 mM) for a period of time to form a SAM-modified Au(111) electrode. The electrode was mounted in the electrochemical cell using the meniscus contact technique [44], which means that only the circular working surface of the hemispherical Au(111) electrode touched the solution.

All electrochemical measurements were performed using an impedance system (EGG, Princeton Applied Research) including a model 283 potentiostat/galvanostat and a model 1025 lock-in amplifier, which were controlled by Power CV and Power Sine software from EG&G PAR on an IBM computer.

To obtain cyclic voltammograms (CVs), the voltage was scanned between −0.20 V and 0.90 V at 20 mV s^{-1}. For EIS measurements, a small sinusoidal perturbation of 5 mV (rms) was applied to the electrode under potentiostatic control and the frequency range was 0.1 Hz–10 kHz. Impedance data were analyzed by nonlinear least squares (NLLS) fitting algorithm using the EQUIVCRT program written by Boukamp [45].

EC STM measurements

In situ STM observations of the Au(111)/solution interface were carried out with a Nanoscope E from Digital Instruments (Santa Barbara, CA). All STM images shown here were acquired in the constant-current mode and presented without applying Fourier transformation filters. The tunneling tips were prepared by electrochemical etching of a tungsten wire (0.25 mm in diameter) in 0.6 M KOH and sealed with transparent nail polish to minimize the Faraday current of the tips. A Au(111) single-crystal bead were prepared at the end of a Au wire (99.99% in purity, 0.8 mm in diameter) following the procedure described previously [41, 46], and used for EC STM measurements. Before each measurement, the Au(111) electrode was further annealed in a hydrogen-oxygen flame for about 2 min, and then quenched in hydrogen-saturated Milli-Q water.

After that, the electrode was mounted into the STM cell and covered with either Milli-Q water or 0.1 M $HClO_4$ solution. The transferring and mounting procedure should be as fast as possible in order to minimize contamination. The STM cell used was a standard commercial cell. A platinum wire served as the quasi-reference electrode. However, all potential values in this work were quoted versus SCE.

Results and discussion

Electrochemical measurements

Figure 1 shows cyclic voltammograms of naked and SAM-modified Au(111) electrodes obtained in the potential range from −0.20 V to 0.90 V, which is within the double-layer potential region of Au(111) electrode [41], at a scan rate of 20 mV/s in 1.0 mM $Fe(CN)^{4-/3-}$ + 0.1 M $HClO_4$ solution. As can be seen from Fig. 1, a pair of well-defined redox waves was observed. Since the redox system used in the present study is not attached to the SAM, mass transfer is involved in the electron transfer reaction at the SAM/solution interface. In the case of fast electron transfer reactions, mass transport is the rate limiting process in the absence of the SAM [14].

At the bare Au(111) electrode, the peak-to-peak separation potential ΔE_p was ~60 mV, showing that the electrode process is reversible [47] and the redox reaction for $Fe(CN)^{4-/3-}$ couple is a diffusion limited reaction in the potential range of interest.

Comparing the cyclic voltammogram at a bare Au(111) with that at a modified electrode (dotted line in Fig. 1), it can be seen that the modification of V-ape-V molecules on Au(111) retards the electron transfer reaction of $Fe(CN)_6^{4-/3-}$ at the electrode surface; the monolayer blocks access to the electrode surface and so reduces the electron transfer rate. As a result, more negative potentials are required to drive the reduction process; or, more positive potentials are required to drive the oxidation process to the diffusion limit [48]. After 20 min modification, the anodic peak-current decreased from 0.66 to 0.63 mA/cm^2, and the cathodic peak-current decreased from −0.65 mA/cm^2 to −0.55 mA/cm^2, respectively.

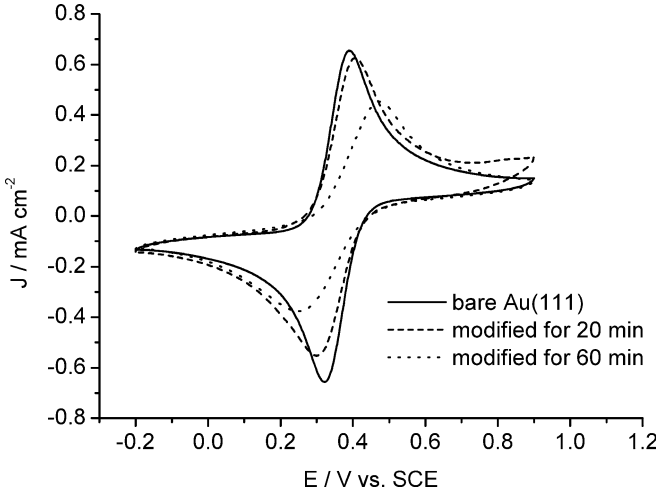

Fig. 1 Cyclic voltammograms for bare and V-ape-V SAM modified Au(111) electrodes in 1.0 mM $Fe(CN)_6^{4-/3-}$ + 0.1 M $HClO_4$ solution. Scan rate is 20 mV/s

As the modification time was increased to 1 h, the electrochemical processes became quasi-reversible [47]. The peak-to-peak potential separation increased to 180 mV, while the peak currents further reduced, indicating an apparent decrease in the rate of the heterogeneous electron-transfer step. It was also observed that further extending the modification time for Au(111) immersed in V-ape-V assembling solution does not significantly influence the blocking effect of the adlayer, indicating that the V-ape-V molecules were adsorbed and self-organized well on Au(111) surface in 0.1 M $HClO_4$ within 1 h.

Figure 2 shows the impedance spectrum in a Nyquist presentation obtained at both bare and V-ape-V SAM modified Au(111) electrodes in 1.0 mM $Fe(CN)^{4-/3-}$ + 0.1 M $HClO_4$ solution. The data were collected at 0.35 V, the formal potential of the investigated redox couple (taken as mid-potential between the anodic and cathodic peaks, as shown in Fig. 1). The equivalent circuits that we used to model the bare Au(111)/solution and Au(111)/SAM/solution systems are shown in Fig. 3. In this figure, R_s is the solution resistance; R_{SAM} represents the resistance of the monolayer to a species moving through the SAM film. R_{ct} is the charge-transfer resistance for the $Fe(CN)^{4-/3-}$ couple at the electrode surface, which corresponds to the diameter of the semicircle in the higher frequency domain of the impedance plots. The parameter Z_W accounts for the Warburg impedance due to the reaction sites. Since a dispersing effect [15, 49, 50] exists for the electrochemical system of Au(111)/V-ape-V-SAM/solution, the constant phase element (CPE, also denoted as Q), which corresponds to the double-layer capacitance at the electrode/solution interface, was used instead of the ideal capacitor in every fit in order to improve the final fit and to minimize error. The complex impedance of the CPE is defined as

$$Z_{CPE} = \frac{1}{Y_0}(j\omega)^{-n}$$

where $j=(-1)^{1/2}$, ω is the angular frequency, Y_0 is a constant and n may vary between −1 and 1. When $n=1$ the above equation represents pure capacitive behavior and $Y_0 = C_{dl}$. In addition, the CPE may represent a semi-infinite Warburg impedance when $n=0.5$ and pure resistance when $n=0$.

For the impedance spectrum observed with bare Au(111) (Fig. 2a), the electrode process is mass transport limited, which was obviously indicated by the 45° Warburg line over the whole measuring frequency range (0.1–10 kHz).The equivalent circuit ($R_s(Q(R_{ct}W))$)

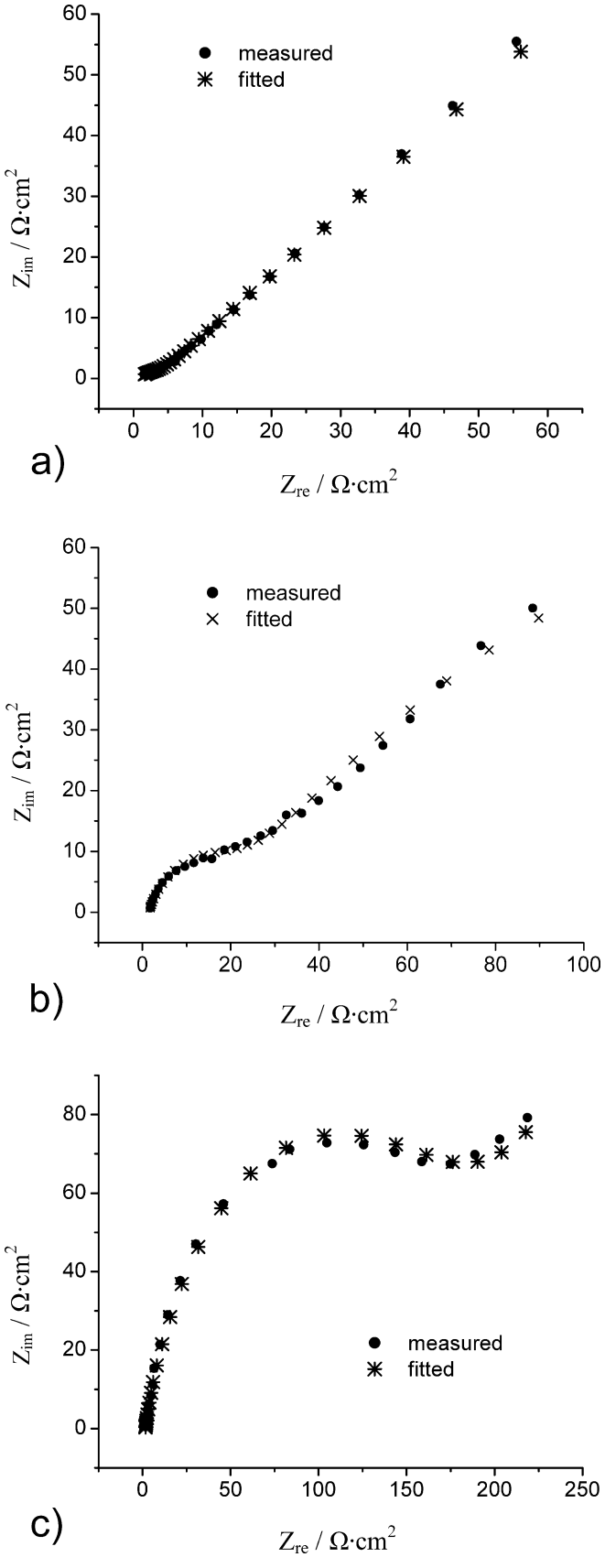

Fig. 2 Electrochemical impedance spectroscopy for bare and V-ape-V SAM modified Au(111) electrodes in 1.0 mM $Fe(CN)_6^{4-/3-}$ + 0.1 M $HClO_4$ solution. **a** bare electrode; **b** immersion for 20 min; **c** immersion for 60 min. The frequency range was 0.1 Hz–10 kHz, and the electrode potential was 0.35 V

which describes this behavior is given in Fig. 3a. There is no R_{SAM} element in this case because there is no SAM present. The simulated plot based on this model agrees well with the experimental results (see Fig. 2), thereby confirming that the analysis is reasonable and accurate.

Figure 2b and c show results from impedance spectroscopy at modified Au(111) electrodes, which are dramatically different from Fig. 2a. A considerable separation in frequencies between the kinetic semicircle and the 45° diffusion region is observed compared to the bare one. The main characteristic feature of the curves measured on the SAM modified Au(111) electrode is the passivating behavior of the V-ape-V monolayers against the reoxidation of $Fe(CN)_6^{4-/3-}$, which is revealed by the circular arc in the higher frequency range. The proposed equivalent circuit ($R_s(QR_{SAM}(R_{ct}W))$) that is capable of describing the impedance data in the presence of a slow electron transfer process is shown in Fig. 3b. The fitted Nyquist diagrams nearly coincide with the measured ones (Fig. 2), and the calculated parameters are listed in Table 1.

From Table 1 we can see that the electron transfer resistance (R_{ct}) at the V-ape-V modified Au(111) electrode can be two orders higher than that at bare Au(111). On the other hand, with the modification time prolonged from 20–60 min, the film resistance (R_{SAM}) increased from 3.47×10^2 Ωcm^2 up to an extremely high value of 1.99×10^{18} Ωcm^2, revealing that the V-ape-V molecules were assembled well, packed densely within 1 h, and can retard the reactive species passing through effectively. The increase in n from 0.56 for bare Au(111) to 0.84 for modified Au reflects the change in the surface electrode process from Warburg diffusion to capacitive behavior. It can be seen that the result obtained from EIS measurements agrees well with that from CV tests.

Electrochemical STM

Ordered structures of V-ape-V adlayers on Au(111) in 0.1 M $HClO_4$ were investigated by electrochemical STM, which is capable of providing insight into the molecular structure. A well-defined terrace-step topography is easily observed on the well-prepared Au(111) surface. The atomic image of Au(111)–(1×1) can be discerned on the terrace in 0.1 M $HClO_4$ solution as reported previously [41].

After examination of the bare Au(111) surface by STM, a droplet of saturated aqueous solution of V-ape-V was injected directly into the STM cell under potential control within the double-layer potential

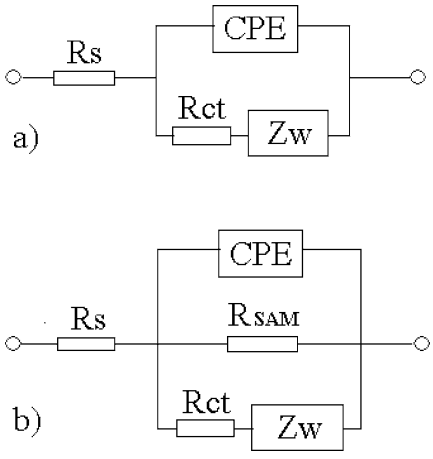

Fig. 3 Electrical equivalent circuits used in this work to fit to the measured impedance data

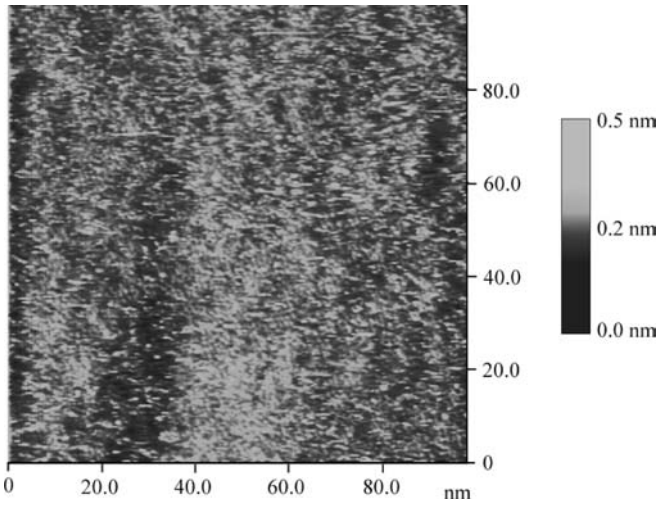

Fig. 4 STM image obtained shortly after adsorption; V-ape-V molecules are randomly distributed on Au(111) surface at this stage. Sample potential was 0.34 V; tunneling current was 0.33 nA; scan rate was 12.2 Hz

region for Au(111) in 0.1 M $HClO_4$ (approximately −0.2∼0.6 V). The Shiff base molecules are adsorbed and self-assembled on Au(111). Initially, the individual molecules are randomly distributed on the surface. Figure 4 was obtained at ∼15 min after adsorption. Imaging the molecules is usually difficult because the adlayer is very disordered and uneven at this stage. This corresponds to weaker blocking ability, as revealed above in electrochemical measurements. After waiting for about one more hour, an ordered monolayer gradually appears. Figure 5 is a typical large-scale STM image acquired at 0.15 V and after ∼1.5 h adsorption. A pair of arrows is used to indicate the <110> and <121> directions of the Au(111) lattice. The monolayer has a high degree of long-range order with few defects in it. The bright stripes seen in Fig. 5a manifest the occurrence of the $(23 \times \sqrt{3})$ reconstruction of the under-lying Au(111) surface. They pair, forming the double-row reconstruction lines as clearly indicated in the section analysis plot shown in Fig. 5b. This feature is identical to that observed previously [19]. The stripes can be used to establish the crystallographic orientation of the substrate, since they are aligned with the <121> direction of the Au(111) surface [27, 51, 52, 53]. There are several possible reasons for the occurrence of the Au(111)–$(23 \times \sqrt{3})$ reconstruction, such as the applied potentials to the substrate, the preparation and pretreatment procedure for the Au(111) electrode, and the adsorption of V-ape-V on the Au(111) surface, and so on. But at the present stage, we can not clarify the exact reason for the observed Au(111) surface reconstruction in this work.

Higher resolution STM images revealed the structural details of the V-ape-V monolayer. Figure 6a shows a STM image resolved at the molecular level, from which it can be seen that the adlayer consists of regular clusters appearing in rectangular shaped bright dots. There are four dots in a cluster, as indicated by x, x', y, y'. The distance between x and x', or between y and y', is 1.10 ± 0.05 nm, and that between x and y, or between x' and y', is 0.90 ± 0.05 nm, respectively, which are close to the corresponding spacings (1.08 nm, and 0.81 nm, respectively) between the four aromatic rings in a V-ape-V molecule. So each cluster in Fig. 6a corresponds to one Shiff base molecule, which is adsorbed onto the Au(111) surface with a flat-lying conformation so as to maximize the interaction between π electrons in V-ape-V and the substrate. On the other hand, the intermolecular spacing in the direction indicated by the arrow AB in Fig. 6a was found to be 1.45 ± 0.05 nm, and that in direction AC was 1.04 ± 0.05 nm. The angle between AB and AC was $\sim 100 \pm 4°$.

Based on the above observation, and regarding the reconstructed Au(111) surface as a quasi-hexagonal structure for simplifications sake, as done by others [41,

Table 1 Characteristic parameters obtained by NLLS regression analysis for the impedance spectroscopy shown in Fig. 2

Electrode	CPE		R_{SAM} (Ωcm^2)	R_{ct} (Ωcm^2)	Z_w
	Y_0 ($\Omega^{-1}cm^{-2}s^n$)	n			
Bare Au(111)	1.81×10^{-3}	0.56	–	3.77	1.22×10^{-2}
20 min immersion	3.19×10^{-4}	0.78	3.47×10^{2}	23.2	8.79×10^{-3}
60 min immersion	5.53×10^{-4}	0.84	1.99×10^{18}	181.0	1.31×10^{-2}

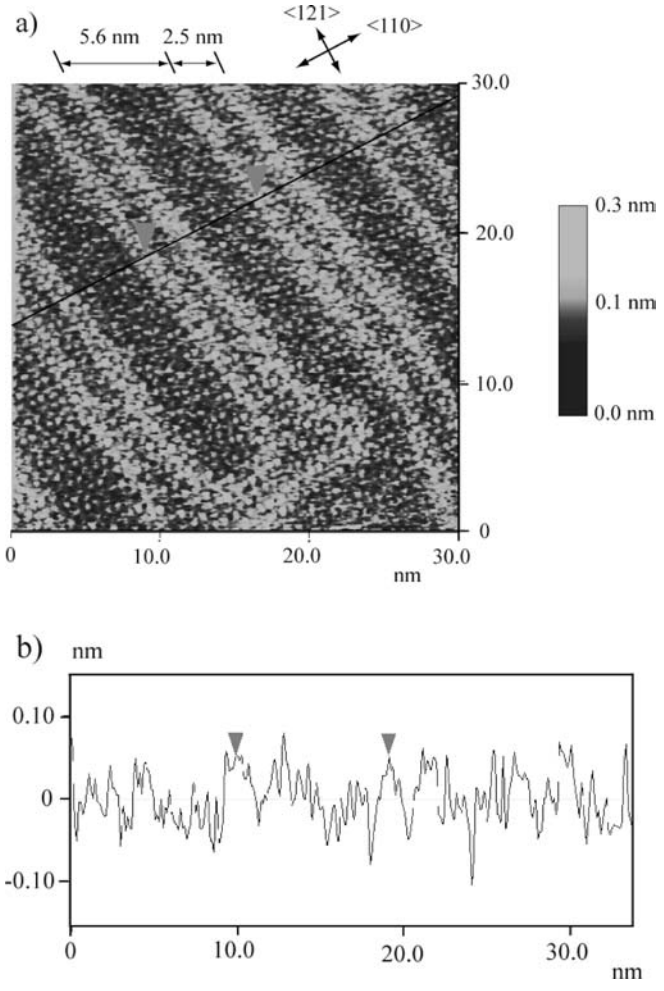

Fig. 5 **a** Low-resolution STM image of Schiff base SAM covered Au(111) surface exhibiting the $(23 \times \sqrt{3})$ reconstruction. Tunneling parameters: $E = 0.15$ V; $I = 5.0$ nA; $f = 12.2$ Hz. **b** The cross-sectional profile along the straight line shown in **a**, illustrating the double-row characteristics of the surface reconstruction

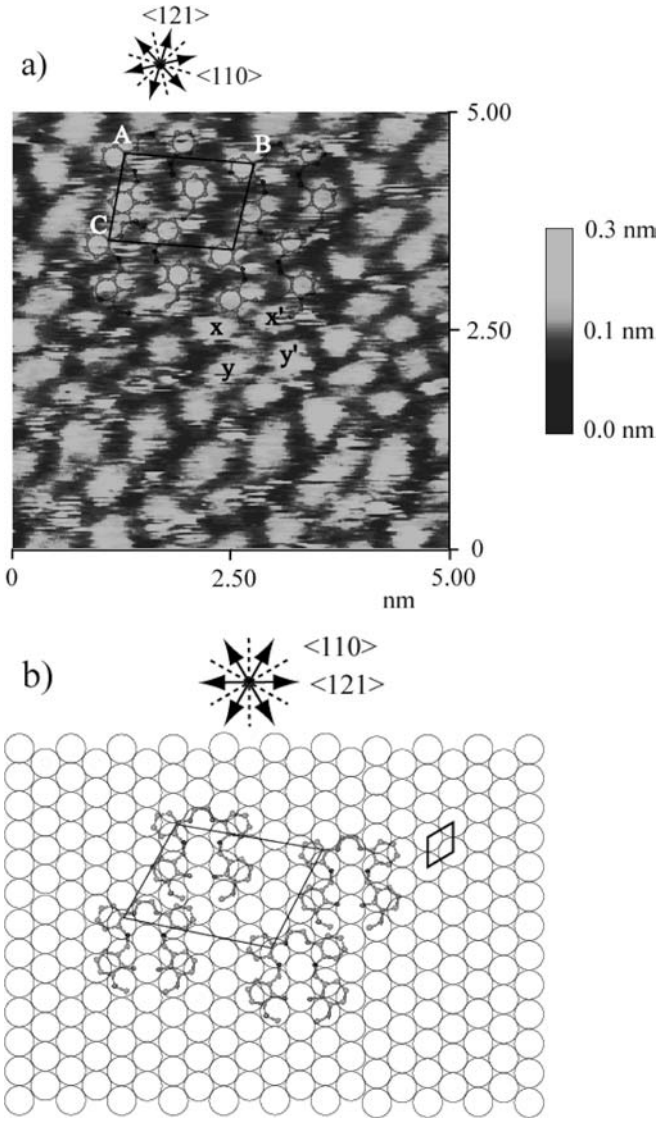

Fig. 6 **a** High-resolution STM image of V-ape-V adlayer on Au(111) surface acquired at 0.33 V. Tunneling current was 0.73 nA. Scan rate was 24.4 Hz. **b** Schematic representation of the adlayer structure

54, 55], a tentatively proposed model for the V-ape-V SAM on Au(111) is depicted in Fig. 6b. The unit cell structure is $(2\sqrt{3} \times 2\sqrt{7})$ symmetric and with a molecular coverage (area per molecule) of 1.44 nm^2/molecule. This structure of the V-ape-V adlayer on Au(111) is different from that observed previously [41], but the molecular coverage is the same. The structural deviation can be understood in the following way. On the one hand, the V-ape-V molecule contains ether bonds (–O–CH_2CH_2–O–), which make the molecule flexible to some extent. On the other hand, compared to the underlying Au atomic lattice, the V-ape-V molecule is large enough to adopt a different orientation when adsorbed. Similar situations have been reported in the literature for other molecules such as L-cysteine on Au(111) [56, 57, 58], for example. The ordered adlayer shown in Figs. 5 and 6 could be imaged within the potential range −0.2–0.6 V, which is within the double-layer potential region in 0.1 M $HClO_4$.

Conclusions

The passivating properties and structures of SAMs of the Shiff base V-ape-V on the surface of Au(111) were investigated in 0.1 M $HClO_4$ solution by CV, EIS, and in situ STM techniques. It was demonstrated that the adsorption of V-ape-V molecules yields a 2-D ordered monolayer with a $(2\sqrt{3} \times 2\sqrt{7})$ unit cell, which is different from that observed previously but has the same molecular coverage. The adlayer provides effective blocking against the reoxidation of the $Fe(CN)^{3-}$/$Fe(CN)_6^{4-}$ couple at the modified electrodes. The electron transfer resistance (R_{ct}) at the SAM modified electrode, obtained from the impedance simulation, is two order of magnitudes higher than that at bare Au(111). The electrochemical reaction of $Fe(CN)_6^{4-/3-}$

becomes quasi-reversible at SAM modified Au(111), while it is typically reversible at the bare one.

Acknowledgements The financial support from the National Natural Science Foundation of China (No. 20303011) is gratefully acknowledged.

References

1. Schreiber F (2000) Prog Surf Sci 65:151
2. Ulman A (1996) Chem Rev 96:1533
3. Finklea HO (2000) Self-assembled monolayers on electrodes. In: Meyers RA (ed) Encyclopedia of analytical chemistry/electroanalytical methods. Wiley, Chichester, UK, pp 1–26
4. Itaya K (1998) Prog Surf Sci 58:121
5. Laibinis PE, Whitesides GM (1992) J Am Chem Soc 114:9022
6. Abbott NL, Rolison DR, Whitesiders GM (1994) Langmuir 10:2672
7. Ramachandran S, Tsai B-L, Blanco M, Chan H, Tang Y, Goddard WA (1996) Langmuir 12:6419
8. Lee S, Puck A, Graupe M, Colorado R, Shon Y-S, Lee TR, Perry SS (2001) Langmuir 17:7364
9. Krysinski P, Moncelli MR, Tadini-Buoninsegni F (2000) Electrochim Acta 45:1885
10. Li H-Q, Chen A, Roscoe SG, Lipkowski J (2001) J Electroanal Chem 500:299
11. Sabatani E, Rubistein I (1987) J Electroanal Chem 219:365
12. Quan Z, Chen S, Li S (2001) Corros Sci 43:1071
13. Feng Y, Teo W-K, Siow K-S, Gao Z, Tan K-L, Hsieh A-K (1997) J Electrochem Soc 144:55
14. Protsailo LV, Fawcett WR (2000) Electrochim Acta 45:3497
15. Bisquert J, Garcia-Belmonte G, Fabregat-Santiago F, Bueno PR (1999) J Electroanal Chem 475:152
16. Sabatani E, Rubinstein I (1987) Phys Chem 91(27):6663
17. Kolb DM (2001) Angew Chem Int Ed 40(7):1162
18. Kong D-S, Chen S-H, Wan L-J, Han M-J (2003) Langmuir 19(6):1954
19. Gewirth AA, Niece BK (1997) Chem Rev 97(4):1129
20. Zamborini FP, Crooks RM (1998) Langmuir 14(12):3279
21. Eliadis ED, Nuzzo RG, Gewirth AA, Alkire RC (1997) J Electrochem Soc 144(1):96
22. Gao X, Weaver MJ (1994) J Electroanal Chem 367:259
23. Nuzzo RG, Korenic EM, Dubois LH (1990) J Chem Phys 93(1):767
24. Dubois LH, Zegarski BR, Nuzzo RG (1993) J Chem Phys 98(1):678
25. Laibinis PE, Whitesides GM, Allara DL, Tao Y-T, Parikh AN, Nuzzo PG (1991) J Am Chem Soc 113(19):7152
26. Poirier GE, Tarlov MJ (1994) Langmuir 10(9):2853
27. Poirier GE (1997) Chem Rev 97(4):1117
28. Touzov I, Gorman CB (1997) J Phys Chem B 101(27):5263
29. Strong L, Whitesides GM (1988) Langmuir 4(3):546
30. Kumar A, BieBuyck HA, Abbott NL, Whitesides GM (1992) J Am Chem Soc 114(23):9188
31. Camillone N, Chidsey CED, Liu G, Scole G (1993) J Chem Phys 98(4):3503
32. Camillone N, Chidsey CED, Liu G, Scole G (1993) J Chem Phys 98(5):4234
33. Gerdy JJ, Goodard WA (1996) J Am Chem Soc 118(13):3233
34. Hautman J, Klein ML (1989) J Chem Phys 91(8):4994
35. Jiang S (2002) Mol Phys 100(14):2261
36. Li S, Chen S, Lei S, Ma H, Yu R, Liu D (1999) Corros Sci 41:1273
37. Li SL, Wang YG, Chen SH, Yu R, Lei SB, Ma HY, Liu DX (1999) Corros Sci 41:1769
38. Quan Z, Wu X, Chen S, Zhao S, Ma H (2001) Corros Sci 57(3):195
39. Quan Z, Chen S, Li Y, Cui X (2002) Corros Sci 44:703
40. Bilgic S, Caliskan N (2001) J Appl Electrochem 31:79
41. Kong D-S, Wan L-J, Han M-J, Pan G-B, Lei S-B, Bai C-L, Chen S-H (2002) Electrochim Acta 48(4):303
42. Honbo H, Sugaware S, Itaya K (1990) Anal Chem 62(22):2424
43. Trevor DJ, Chidsey CED, Loiacono DN (1989) Phys Rev Lett 62(8):929
44. Hamelin A (1985) In: Conway BE, White R, Bockris JO'M (ed) Modern aspects of electrochemistry, Vol 16. Plenum, New York, Ch 1
45. Boukamp BA (1993) Equivalent circuits (v4.55), users manual, 2nd edn. University of Twente, Netherlands
46. Wan L-J, Terashima M, Noda H, Osawa M (2000) J Phys Chem B 104(15):3563
47. Bard AJ, Faulkner LR (2001) Electrochemical methods: fundamentals and applications, 2nd edn. Wiley, New York, Ch 6, pp 226
48. Chidsey CED, Loiacono DN (1990) Langmuir 6(3):682
49. Ma H, Chen S, Cheng X, Chen X, Li G, Yang X (1997) J Serb Chem Soc 62(12):1201
50. Wrona PK, Lasia A, Lessard M, Menard H (1992) Electrochim Acta 37(7):1283
51. Sandy AR, Mochrie SGJ, Zehner DM, Huang KG, Gibbs D (1991) Phys Rev B 43(6):4667
52. Wöll C, Chiang S, Wilson RJ, Lippel PH (1987) Phys Rev B 39(11):7988
53. Liu YB, Sun DY, Gong XG (2002) Surf Sci 498:337
54. Poirier GE (1999) Langmuir 15(4):1167
55. Gao X, Edens GJ, Weaver MJ (1994) J Phys Chem 98(33):8074
56. Dakkouri AS, Kolb DM, Edelstein-Shima R, Mandler D (1996) Langmuir 12(11):2849
57. Zhang JD, Chi QJ, Nielsen JU, Friis EP, Andersen JET, Ulstrup J (2000) Langmuir 16:7229
58. Xu Q-M, Wan L-J, Wang C, Bai C-L, Wang Z-Y, Nozawa T (2001) Langmuir 17(20):6203